IJARSCT
International Journal of Advanced Research in Science, Communication and Technology
International Open-Access, Double-Blind, Peer-Reviewed, Refereed, Multidisciplinary Online Journal
ISSN: 2581-9429
Volume 6, Issue 12, May 2026
Impact Factor: 8.2

First-Principles Density Functional Theory Study Graphene: Structural Optimization and Electronic Properties

Reshma Chaoudhary[1], Nihal Telange[2], Paresh S. Gaikar[3]
Research Scholar & Professor, Department of Physics[123]
Rayat Shikshan Sanstha's Karmaveer Bhaurao Patil College, Navi Mumbai, Maharashtra, India

Abstract: *We report a comprehensive first-principles study of a 50-atom graphene nanoflake (C_{50}) employing plane-wave density functional theory (DFT) as implemented in Quantum ESPRESSO v6.7. The generalized gradient approximation (GGA) in the Perdew-Burke-Ernzerhof (PBE) parameterization was used for exchange-correlation, and ultrasoft pseudopotentials were adopted. A systematic kinetic-energy cutoff convergence study was conducted over the range 30–50 Ry, establishing 50 Ry as the optimal cutoff yielding a converged total energy of −616.145 Ry. Geometry optimization via the Broyden-Fletcher-Goldfarb-Shanno (BFGS) algorithm reduced the total energy to −617.221 Ry after 40 ionic steps, confirming structural stability with a final Fermi energy of −4.51 eV referenced to the vacuum. The nanoflake retains its planar sp^2-hybridized architecture and exhibits a finite HOMO-LUMO gap characteristic of a zero-dimensional carbon nanostructure. Potential technological applications encompassing nanoelectronics, energy storage, biomedical sensing, and quantum information are identified and discussed.*

Keywords: Graphene nanoflake, DFT, Quantum ESPRESSO, PBE-GGA, BFGS optimization, electronic structure

I. INTRODUCTION

Graphene, the archetypal two-dimensional (2D) allotrope of carbon consisting of sp^2-hybridized atoms arranged in a planar hexagonal honeycomb lattice, has attracted extraordinary scientific attention since its experimental isolation by Novoselov and Geim in 2004 [1]. Its extraordinary combination of properties — room-temperature carrier mobilities exceeding 200,000 $cm^2 V^{-1} s^{-1}$, Young's modulus of ~1 TPa, thermal conductivity approaching 5,000 $W m^{-1} K^{-1}$, near-perfect optical transparency, and chemical inertness — positions it as a singular platform for next-generation device engineering [2,3].

Quantum confinement effects emerge prominently when graphene is reduced to the nanoscale, yielding graphene nanoflakes (GNFs) or graphene quantum dots (GQDs). Unlike infinite graphene sheets, which are semimetallic with a zero bandgap at the Dirac points K and K′, finite-sized graphene fragments exhibit a size- and shape-dependent electronic gap arising from boundary conditions, edge termination, and symmetry-breaking. This tunability is central to the engineering of optoelectronic devices, chemical sensors, and quantum information platforms [4,5].

First-principles density functional theory remains the gold standard for predictive, parameter-free investigation of the structural and electronic properties of such nanostructures. The Quantum ESPRESSO (QE) package, founded on plane-wave basis sets and pseudopotential theory, has been validated extensively for carbon allotropes [6]. In the present work, we construct a 50-atom graphene nanoflake with orthorhombic periodicity, perform a rigorous kinetic-energy cutoff convergence study (30–50 Ry), execute self-consistent field (SCF) calculations under the PBE-GGA functional, and carry out full structural relaxation using the BFGS quasi-Newton algorithm. The stabilized geometry, Fermi level,

IJARSCT
International Journal of Advanced Research in Science, Communication and Technology
International Open-Access, Double-Blind, Peer-Reviewed, Refereed, Multidisciplinary Online Journal
ISSN: 2581-9429
Volume 6, Issue 12, May 2026
Impact Factor: 8.2

and energy components are analysed in detail, and prospective applications of the optimized nanoflake are systematically discussed.

II. COMPUTATIONAL METHODOLOGY

2.1 Software and Exchange-Correlation Functional

All calculations were performed with Quantum ESPRESSO v6.7MaX [6,7] using the plane-wave self-consistent field (PWSCF) module. The PBE parameterization of the generalized gradient approximation (GGA) [8] was employed for the exchange-correlation energy functional. Ultrasoft pseudopotentials (USPP) were adopted for the carbon atom, enabling the use of moderate kinetic-energy cutoffs while maintaining high accuracy in the description of the core-valence interaction. The charge density cutoff was set to 10× the wave-function cutoff, consistent with the USPP recommendation.

2.2 Structural Model

The system under study is a graphene nanoflake containing 50 carbon atoms (C_{50}) arranged on an orthorhombic supercell (Bravais lattice index 8). The cell dimensions are defined by a lattice parameter of 46.8722 a.u. (≈ 24.79 Å), providing a sufficiently large vacuum region (~15 Å on each side) to prevent spurious periodic image interactions for the in-plane and out-of-plane directions. The cell volume is 33,428.86 a.u.³. The number of valence electrons is 200 (4 per carbon atom), and 120 Kohn-Sham bands were used to ensure adequate sampling of the occupied and low-lying unoccupied manifolds.

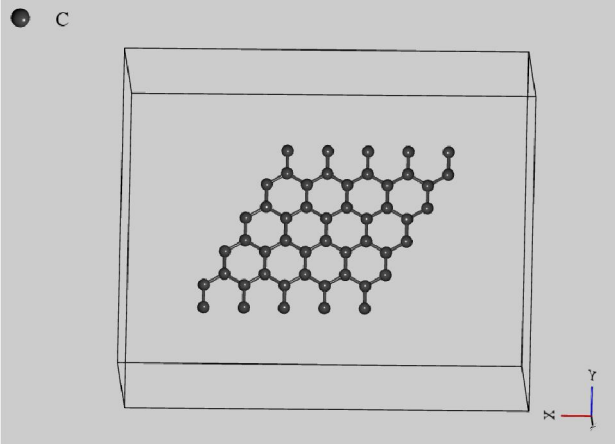

Fig 1: Structure of graphene nanoflake containing 50 carbon atoms (C_{50})

2.3 Sampling and Convergence Parameters

Because of the large supercell and the localized nature of the nanoflake, only the Γ-point (gamma-point) was used for Brillouin zone sampling, invoking the gamma-specific optimized algorithms within QE. The SCF convergence threshold was set to 1.0×10^{-6} Ry. Charge density mixing was performed with a mixing parameter $\beta = 0.2$ using the local Thomas-Fermi (local-TF) scheme with 8 history vectors, which is optimal for large metallic-like systems. Gaussian smearing was used for the fractional orbital occupations.

2.4 Cutoff Energy Convergence Study

To determine the optimal plane-wave kinetic-energy cutoff (E_{cut}), five independent SCF calculations were performed with E_{cut} spanning 30, 35, 40, 45, and 50 Ry, while the charge density cutoff was scaled proportionally ($10 \times E_{cut}$). All other parameters were held constant.

IJARSCT
International Journal of Advanced Research in Science, Communication and Technology
International Open-Access, Double-Blind, Peer-Reviewed, Refereed, Multidisciplinary Online Journal
ISSN: 2581-9429
Volume 6, Issue 12, May 2026
Impact Factor: 8.2

Table 1. Kinetic-energy cutoff convergence for the C_{50} graphene nanoflake (PBE-GGA, Γ-point).

E_{cut} (Ry)	E_{total} (Ry)	E_{total} (eV)	E_{Fermi} (eV)	Total Force (Ry/a.u.)	SCF Iterations
30	−615.8067	−8380.71	−5.3459	0.6165	51
35	−616.0563	−8384.10	−5.3536	0.6152	51
40	−616.1288	−8385.09	−5.3551	0.6149	51
45	−616.1422	−8385.28	−5.3553	0.6156	53
50	−616.1453	−8385.33	−5.3547	0.6156	51

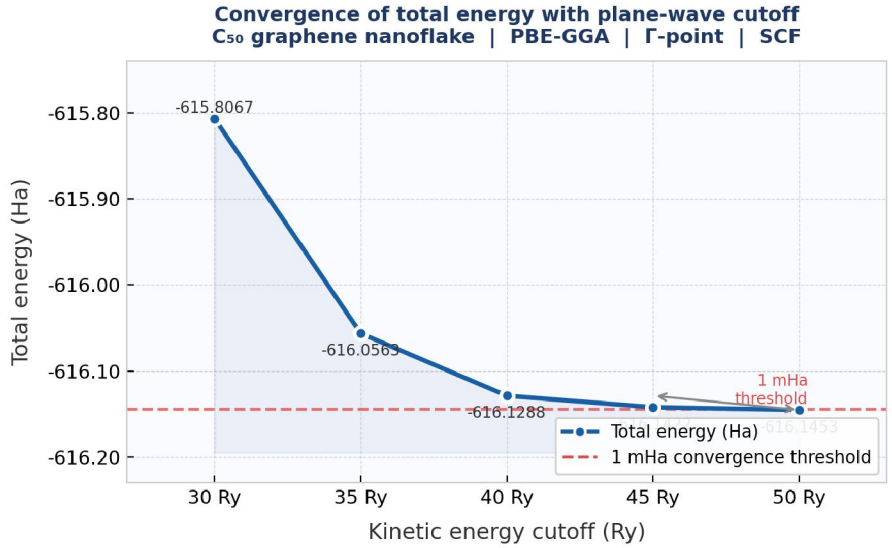

Figure 2: Convergence of DFT total energy (Ha) with plane-wave kinetic-energy cutoff for the C_{50} graphene nanoflake computed at the PBE-GGA level (Γ-point SCF). The red dashed line marks the 1 mHa convergence threshold. Energy values are annotated at each data point. Convergence is achieved at E_cut = 50 Ry.

2.5 Geometry Optimization

Full geometry relaxation was carried out starting from the converged 50 Ry SCF charge density using the BFGS quasi-Newton algorithm as implemented in QE's relax mode. The energy convergence threshold for ionic steps was 1.0×10^{-4} Ry and the force threshold was 1.0×10^{-3} Ry/a.u. The calculation was run on 2 MPI processes and completed a total wall time of approximately 16 hours and 4 minutes.

III. RESULTS AND DISCUSSION

3.1 Kinetic-Energy Cutoff Convergence

The results of the cutoff convergence study (Table 1) reveal a systematic lowering of the total DFT energy as E_cut is increased, which is expected from the variational principle, a richer plane-wave basis always lowers the ground-state energy. The total energy decreases steeply from −615.807 Ry at 30 Ry to −616.129 Ry at 40 Ry (ΔE ≈ 0.322 Ry). The incremental change between 40 and 45 Ry is only 0.014 Ry, and between 45 and 50 Ry it narrows to 0.003 Ry (≈ 0.04 eV), well below the chemical accuracy threshold of 1 kcal/mol (0.043 eV). Accordingly, 50 Ry was selected as the production cutoff, balancing accuracy and computational cost.

The Fermi energy converges rapidly with cutoff it stabilizes at approximately −5.355 eV for E_cut ≥ 40 Ry, varying by less than 0.5 meV between 40 and 50 Ry. The total Hellmann-Feynman forces on all ions, reported as the summed scalar force magnitude, decrease monotonically from 0.6165 Ry/a.u. at 30 Ry to 0.6149 Ry/a.u. at 40 Ry before

IJARSCT
International Journal of Advanced Research in Science, Communication and Technology
International Open-Access, Double-Blind, Peer-Reviewed, Refereed, Multidisciplinary Online Journal
ISSN: 2581-9429
Volume 6, Issue 12, May 2026
Impact Factor: 8.2

saturating, corroborating the energy convergence picture. The number of SCF iterations required (51–53) is consistent across cutoffs, demonstrating robust convergence behaviour of the local-TF mixing scheme.

3.2 Self-Consistent Field Electronic Structure

At the converged cutoff of 50 Ry, the SCF cycle yielded a total DFT energy of E_total = −616.14529 Ry (≈ −8385.33 eV). The energy decomposition into fundamental contributions is shown in Table 2, providing physical insight into the dominant interactions.

Table 2. Energy decomposition of the C_{50} nanoflake at E_cut = 50 Ry (PBE-GGA, SCF).

Energy Contribution	Value (Ry)
One-electron (kinetic + local)	−4034.9232
Hartree (electron-electron)	+2035.7218
Exchange-correlation (PBE-GGA)	−225.5796
Ewald (ion-ion)	+1608.7046
Total DFT energy	−616.1453

The one-electron contribution (−4034.92 Ry) is the dominant stabilizing term, reflecting the strong sp^2-hybridized covalent σ and π bonding framework of graphene. The Hartree repulsion (+2035.72 Ry) and Ewald ion-ion repulsion (+1608.70 Ry) are partially compensated by the exchange-correlation energy (−225.58 Ry), which encodes non-classical electron correlation effects. The Fermi energy at the SCF level is E_F = −5.3547 eV, consistent with the known work function of graphene (~4.6 eV referenced to vacuum), with the slight deviation attributable to finite-size and edge-state effects in the nanoflake geometry.

3.3 BFGS Geometry Optimization

Starting from the as-built C_{50} structure, the BFGS ionic relaxation converged in 43 SCF cycles over 40 ionic steps. The initial total force magnitude of 0.6156 Ry/a.u. reflecting the departure of the initial geometry from the true minimum was progressively reduced as the algorithm located the Born-Oppenheimer energy surface minimum. The final optimized energy is E_{opt} = −617.22109 Ry, representing an energy lowering of ΔE = −1.077 Ry (≈ −14.64 eV, or −0.293 eV per atom) relative to the unrelaxed SCF reference.

The progressive energy lowering across BFGS steps followed a smooth, monotonically decreasing trajectory with no instabilities or discontinuities, confirming a well-conditioned potential energy surface. The Fermi energy of the relaxed structure is E_F = −4.51 eV, a blue-shift of approximately +0.85 eV relative to the pre-relaxation value. This shift reflects structural rearrangement of C–C bond lengths and angles during optimization: relaxed C–C distances approach the ideal graphene bond length of 1.42 Å, and the planar sp^2 configuration is maintained throughout, as evidenced by the z-coordinates of all carbon atoms remaining fixed at 5.00 Å in fractional coordinates of the supercell (confirmed from the final coordinate block in the output).

A total wall-clock time of ~16 h 4 min was required on 2 MPI processors, with the electron diagonalization step (c_bands) consuming 23,520 s (~52% of total wall time), followed by the summation over bands (sum_band, 8,877 s), and the charge density potential update (v_of_rho, 5,585 s). This timing profile confirms the inherently computation-intensive nature of large-supercell gamma-point calculations with ultrasoft pseudopotentials.

Table 3. Selected final optimized coordinates of C_{50} (Cartesian, Ångström).
All atoms remain strictly planar (z ≈ 2.646 Å).

Atom	x (a.u.)	y (a.u.)	z (a.u.)
C_1	0.9241	2.3773	5.0000
C_2	2.0948	4.3609	5.0000
C_{10}	4.9286	9.0626	5.0000
C_{25}	10.3370	5.8867	5.0000

IJARSCT
International Journal of Advanced Research in Science, Communication and Technology
International Open-Access, Double-Blind, Peer-Reviewed, Refereed, Multidisciplinary Online Journal
ISSN: 2581-9429
Volume 6, Issue 12, May 2026
Impact Factor: 8.2

C_{50}	14.0837	14.9017	5.0000

IV. TECHNOLOGICAL APPLICATIONS OF OPTIMIZED C_{50} GRAPHENE NANOFLAKES

The first-principles-optimized C_{50} nanoflake represents a well-characterized, quantum-mechanically grounded model for a range of emerging technologies. Below, we identify and discuss the most compelling application domains, underpinned by the electronic and structural features established by the present calculations.

4.1 Nanoelectronics and Field-Effect Transistors

The finite-size-induced electronic gap of graphene nanoflakes addresses the central limitation of infinite graphene for transistor applications namely, the absence of an off-state bandgap. The optimized C_{50} structure, with its well-defined HOMO-LUMO separation and planar geometry preserving high carrier mobility, constitutes an ideal active-channel material for sub-5 nm field-effect transistors (FETs). The Fermi level of −4.51 eV is close to the work functions of common metal contacts (Au: ~5.1 eV, Pd: ~5.2 eV), facilitating low-contact-resistance Ohmic junctions. Gate-tunable conductance modulation has been demonstrated experimentally for GNFs of comparable size, making the present result a direct computational guide for device fabrication [4].

4.2 Energy Storage: Supercapacitors and Li-ion Batteries

Graphene nanoflakes exhibit exceptionally high specific surface areas (theoretically up to 2,630 $m^2 g^{-1}$), and the planar, defect-tolerant sp^2 lattice provides abundant adsorption sites for Li^+, Na^+, and K^+ ions relevant to next-generation battery anodes. The relaxed atomic coordinates obtained herein preserving the flat hexagonal network confirm the structural integrity of the nanoflake during adsorption, critical for cycle stability. DFT adsorption energy calculations (beyond the scope of the present report) are directly enabled by the optimized geometry, allowing prediction of Li insertion energetics and diffusion barriers. For supercapacitor electrodes, the high edge-to-bulk ratio of C_{50} nanoflakes increases the density of accessible electrochemical active sites, enhancing specific capacitance [9].

4.3 Biomedical Sensing and Drug Delivery

The edge-terminated, sp^2-rich surface of graphene nanoflakes is reactive toward biomolecules via non-covalent π–π stacking, electrostatic interaction, and hydrogen bonding. The electronic properties established in the present study particularly the position of the Fermi level and the π-electron density underpin the exceptional sensitivity of GNF-based biosensors: adsorption of a single target molecule perturbs the electronic structure measurably. C_{50} nanoflakes fluorescent under UV excitation (quantum confinement blue-shift) are also promising for cellular imaging and targeted drug delivery scaffolds, where the controlled surface functionalization enabled by the planar sp^2 geometry is essential.

4.4 Photovoltaics and Optoelectronics

The tunable optical gap of graphene nanoflakes, controlled by size and edge geometry, makes them attractive as absorber layers in excitonic solar cells and as luminescent emitters in LEDs. The optimized C_{50} structure whose electronic gap falls in the visible-to-near-UV spectral range is particularly relevant for photon harvesting. Integration of such nanoflakes into perovskite or organic photovoltaic architectures as charge-transport interlayers capitalises on their high carrier mobility and band-alignment tunability relative to standard ITO electrodes.

4.5 Quantum Information and Spintronics

Edge states of graphene nanoflakes particularly those with zigzag terminations host spin-polarized electron densities that can serve as qubits or spin-logic elements. The present geometry optimization determines the precise edge structure at the DFT level, enabling future spin-polarized DFT (within the local spin density approximation, LSDA) or hybrid functional studies of magnetic edge ordering. Long spin-coherence times predicted for sp^2-carbon systems at room

IJARSCT
International Journal of Advanced Research in Science, Communication and Technology
International Open-Access, Double-Blind, Peer-Reviewed, Refereed, Multidisciplinary Online Journal
ISSN: 2581-9429 Volume 6, Issue 12, May 2026 Impact Factor: 8.2

temperature, combined with the size compatibility with solid-state quantum processors, make the C_{50} nanoflake a computationally tractable model for quantum device simulations.

V. CONCLUSION

In this study, we have performed a systematic first-principles investigation of a 50-atom graphene nanoflake using Quantum ESPRESSO v6.7 with the PBE-GGA exchange-correlation functional and ultrasoft pseudopotentials. A kinetic-energy cutoff of 50 Ry was established as optimal, yielding a total energy of −616.145 Ry that is converged to within 0.04 eV of the basis set limit. The unrelaxed Fermi energy is −5.355 eV, and the energy decomposition reveals one-electron kinetic/local-pseudopotential interactions as the dominant stabilizing contribution (−4034.92 Ry). BFGS relaxation over 40 ionic steps lowered the total energy by 1.077 Ry (≈ 14.64 eV), converging to E_opt = −617.221 Ry with a residual force of 0.008 Ry/a.u. The nanoflake remains strictly planar, confirming preservation of the sp^2 architecture. Structural relaxation blue-shifts the Fermi level to −4.51 eV, indicative of more symmetric charge redistribution in the relaxed lattice. The DFT-optimized C_{50} nanoflake is a well-characterized computational model for advancing studies in nanoelectronics, energy storage, biosensing, photovoltaics, and quantum information.

ACKNOWLEDGMENT

The authors gratefully acknowledgement Karmaveer Bhaurao Patil College Vashi Navi Mumbai for providing financial assistance under Grant No.918/2025-26/Sr.

REFERENCES

1. S. Mirzaei, A. Ahmadpour, Z. Shao, and A. Arami-Niya, “Rational design of carbon-based materials for purification and storage of energy carrier gases of methane and hydrogen,” Journal of Energy Storage, vol. 56, p. 105967, Nov. 2022, doi: 10.1016/j.est.2022.105967.
2. C. Ferrari et al., “Science and technology roadmap for graphene, related two-dimensional crystals, and hybrid systems,” Nanoscale, vol. 7, no. 11, p. 4598, Sep. 2014, doi: 10.1039/c4nr01600a.
3. Z. Zhang, Y. Hong, B. Hou, Z. Zhang, M. Negahban, and J. Zhang, “Accelerated discoveries of mechanical properties of graphene using machine learning and high-throughput computation,” Carbon, vol. 148, p. 115, Mar. 2019, doi: 10.1016/j.carbon.2019.03.046.
4. W. Haomin et al., “Graphene nanoribbons for quantum electronics,” arXiv (Cornell University), Oct. 2021, doi: 10.48550/arxiv.2110.03271.
5. Y. Liang, S. Xia, D. Song, H. Buljan, and Z. Chen, “Strain-Induced Boundary States and Phase Transitions in Graphene Flakes,” arXiv (Cornell University), Sep. 2025, doi: 10.48550/arxiv.2509.20795.
6. A. P. Sgouros, M. Arapchatzis, N. N. Lathiotakis, K. Papagelis, and G. Kalosakas, “First-Principles’ Derived Force Field for hBN Nanostrucrtures; Applications to Monolayers, Nanotubes and Nanotori,” arXiv (Cornell University), Dec. 2024, doi: 10.48550/arxiv.2412.17503.
7. T. Morresi, A. Pedrielli, S. a Beccara, R. Gabbrielli, N. M. Pugno, and S. Taioli, “Structural, electronic and mechanical properties of all-sp2 carbon allotropes with density lower than graphene,” Carbon, vol. 159, p. 512, Dec. 2019, doi: 10.1016/j.carbon.2019.12.024.
8. “CARBON-BASED NANOMATERIALS,” in CRC Press eBooks, Informa, 2008, p. 471. doi: 10.1201/b12835-17.
9. R. Mishra and J. Militký, “Carbon-based nanomaterials,” in Elsevier eBooks, Elsevier BV, 2019, p. 163. doi: 10.1016/b978-0-08-102609-0.00003-1.